Bidensity Particle-Laden Slurries on an Incline: Experimental Investigation of Constant Volume and Constant Flux Conditions

Dominic Diaz[1], **Aviva Prins, Jessica Bojorquez, Josh Crasto, Margaret Koulikova, Tameez Latib, Andrew Shapiro, and Clover Ye**

Mentors: David Arnold, Claudia Falcon, Michael Lindstrom, and Andrea Bertozzi

Department of Mathematics, University of California, Los Angeles

October 16, 2018

Abstract

Particle-laden slurries are pervasive in both natural and industrial settings, whenever particles are suspended or transported in a viscous fluid. Previous literature has studied constant volume monodisperse and bidensity slurries, with negatively buoyant particles, on an incline. It has been shown that these slurries form three distinct regimes depending on the fraction of particles and inclination angle. The three regimes are: settled (where particles settle to the bottom of the mixture and the suspending fluid separates from and moves faster than the settled particles), well-mixed (where particle concentration is constant throughout the slurry), and ridged (where particle concentration is largest at the front of the fluid and a tall leading ridge forms). Here we experimentally study the flow of bidensity slurries on an incline in the constant volume case and the constant flux case while varying three parameters—inclination angle α, total particle volume fraction ϕ, and particle volume fraction ratio χ. We find that for both types of initial conditions, small ϕ and α result in a settled regime and high ϕ and α result in a ridged regime. Intermediate values of these two parameters are shown to produce a well-mixed regime. We additionally show that our experimentally found front positions for both conditions show loose agreement with theoretical predictions. Height profiles (film thicknesses) are also presented, which show that the ridged regime has a distinct profile from the other two regimes.

Keywords: thin films, particle-laden flow, multiphase fluids, interfacial flows

1. Introduction

A particle-laden slurry is a mixture of particles suspended in a viscous fluid. Studies of the dynamics of slurries became increasingly popular after Huppert [4] published his findings involving the flow of a thin film of viscous fluid down an incline. Since then, much work has been done to examine the flow of thin films of viscous fluid with a single particle species suspended within the flow (called monodisperse slurries). This topic has been explored both theoretically

[1]All correspondence should be sent to: dominicdiaz@g.ucla.edu

Mentor information: David Arnold (darnold@math.ucla.edu), Claudia Falcon (cfalcon@math.ucla.edu), and Michael Lindstrom (mikel@math.ucla.edu)

and experimentally in [1, 5, 7, 8, 9, 11, 13], among others. Particle-laden slurries appear in a variety of industrial and natural settings, including spiral particle separators in which materials are processed and separated [2, 12] and landslides [3].

Bidensity particle-laden slurries are mixtures of two species of particles with different densities and similar diameters suspended in a viscous fluid. When on an incline, particles in the mixture experience either sedimentation on the incline surface (due to gravity) or shear-induced migration, which leads particles away from areas of high shear rate and high particle concentration (away from the incline surface). Depending on the relative strength of these two effects, there are three possible regimes that can arise: ridged, well-mixed, and settled. The ridged regime occurs when shear-induced migration dominates gravitational settling, and is identified by a high concentration of particles on the front edge of the fluid, forming a leading ridge. In the settled regime, where gravity dominates shear-induced migration, particles form a sediment at the bottom of the fluid as it flows down the track. Within this regime for a bidensity slurry, separation between different particles and fluid can be observed. The well-mixed regime, a transient state between the other two regimes [9], is formed when neither of these effects dominate and particles stay evenly distributed throughout the fluid. These regimes have been studied in the monodisperse (single particle species) case for a constant volume of fluid in [6, 8, 9, 13] and in the bidensity case for a constant volume of fluid in [10].

Previous research has investigated the relevant characteristics of slurries with constant volume. In 2011, Murisic et al. [9] investigated monodisperse constant volume slurries with varying fluid viscosity and particle diameters. They constructed the regime phase diagram for a specific fluid viscosity and particle diameter with varying particle volume fraction and angle of inclination. The general result presented in [9] is that the ridged regime tends to form for high inclination angle and particle concentration while the settled regime tends to form for small inclination angle and particle concentration. This result comes from the effect of shear-induced migration increasing with greater angle and/or particle concentration. Theory is extended to include bidensity slurries by Lee et al. [11], which compared the bidensity constant volume case with monodisperse constant volume case and derived a model for bidensity constant volume slurries flowing down an incline. The bidensity model for a constant volume of fluid is further extended in [5].

In the current study, we conduct experiments with bidensity slurries flowing down an incline with two different initial conditions: constant volume (where a finite volume of slurry is used) and constant flux (where slurry is pumped at a constant rate at the top of the incline). We consider the results from Lee's model ([11]) for particle distribution normal to the plane of the track for particle-laden slurries flowing down an incline with constant volume. We expect similar phenomena to arise in the constant flux case since while the initial condition and the top boundary condition of the slurry change, the theory in both is the same. While many previous studies focused primarily on front position, we provide additional experimental data for the height of the fluid for the constant flux case.

In order to predict the behavior of constant volume slurries flowing down an incline, various papers have extended the results of [4] which finds that the fluid's average front position evolves with a behaviour asymptotic to $t^{1/3}$ (where t is time) for a thin film of viscous fluid. In both the monodisperse and bidensity case for a finite volume of fluid ([8] and [5], respectively), it has been shown that the average front position is still asymptotic to $t^{1/3}$. We find that our results for the average front position in the constant volume case are in loose agreement with previous literature, but that our results for the constant flux case exhibit distinct behavior for the front position of the fluid from the constant volume case. We also demonstrate how the height of the fluid for the regimes differ.

The paper is organized as follows. In §2 we describe how the experiments were conducted (including what materials were used) and how the data was analyzed. We then present our experimental results and analysis in §3, and conclude our findings in §4.

2. Experimental procedure

2.1. Materials

The mixtures used in our experiments consisted of glass and ceramic beads suspended in a silicone oil. The particles, manufactured by Ceroglass, are described in Table 1. There is a slight disparity in the average diameter of the two particles although we assume that their diameters are the same for the purposes of this paper. For the majority of our constant volume experiments, the particle color originated from the manufacturer. However, in some of the constant volume experiments we dyed clear ceramic beads (with similar properties to the SLZ-2 ceramic beads) red to maintain consistency in the color of the particles used. We did not dye the particles in the constant flux experiments. The viscous fluid we used was polydimethylsiloxane (see the last row of Table 1 for properties).

Material	Density	Color	Other Properties
GSB-7 glass beads	2.5 g/cm^3	white	diameter: 0.18 - 0.25 mm
SLZ-2 ceramic beads	3.8 g/cm^3	red	diameter: 0.125 - 0.25 mm
polydimethylsiloxane (PDMS)	0.971 g/cm^3	clear	kinematic viscosity: 10 cm^2/s

Table 1: Materials used in our experiments. The density and diameter are the same for all experiments. Note that for constant flux experiments, the color of both particles was white.

2.2. Conducting the experiments

In this study we performed a series of experiments on gravity driven bidensity slurries flowing on an incline. We varied four parameters for each experiment: inclination angle of the track α, the volume fraction ratio of lighter density particles (glass) to heavier density particles (ceramic) χ, total particle volume fraction ϕ, and the initial condition (either constant volume or constant flux). We define the volume fraction of glass and ceramic particles respectively as:

$$\phi_g = \frac{V_g}{V_g + V_c + V_f}, \qquad \phi_c = \frac{V_c}{V_g + V_c + V_f}.$$

Where V_g is the volume of glass particles, V_c is the volume of the ceramic particles, and V_f is the volume of fluid in the mixture. We additionally define the total particle volume fraction as the sum of the two particle volume fractions:

$$\phi = \phi_g + \phi_c.$$

We define the volume fraction ratio χ as the ratio of ϕ_g to the total volume fraction, $\phi_g + \phi_c$:

$$\chi = \frac{\phi_g}{\phi_g + \phi_c} = \frac{V_g}{V_g + V_c}.$$

The two initial conditions—constant volume or constant flux—are defined in terms of their nondimensional height by the following two equations, respectively:

$$h(x,t=0)=\begin{cases}0 & \text{if } x<-l\\ 1 & \text{if } -l<x<0\\ 0 & \text{if } x>0\end{cases}, \quad \text{and} \quad h(x,t=0)=\begin{cases}1 & \text{if } x<0\\ 0 & \text{if } x>0,\end{cases} \tag{1}$$

where x and t are nondimensional position and time, respectively. We define l as some nondimensional length, $x=0$ as the location where the slurry starts to flow, and $t=0$ as the time in which the slurry starts to flow. Schematic diagrams of these two initial conditions are presented in Figure 1.

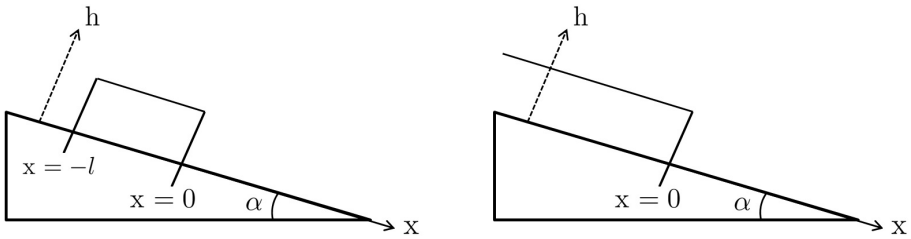

Figure 1: Schematic diagram of the constant volume (left) and constant flux (right) initial conditions.

To perform our experiments, we used an acrylic track (length 90 cm and width 14 cm) with an adjustable angle, α, (see Figure 2) that was modified slightly for each of the two initial conditions: constant volume and constant flux. In the constant volume experiments, the region on the track behind the gate (see Figure 2, left) was filled with 80 mL of well-mixed slurry. The gate was then quickly lifted to allow the slurry to flow down the track. In the constant flux experiments, a weir was placed near the top of our track (see Figure 2, right). On the portion of the track above the weir, we constantly pumped well-mixed slurry onto the track. The purpose of the weir was to ensure that the slurry flowed onto the track evenly along the width of the track (y-axis). The volume of slurry entering the track over time was constant at around 3 cm^3/s for $\phi = 0.25$ experiments and around 0.75 cm^3/s for $\phi = 0.45$ experiments. Thus, the volumetric flux, or flow rate per unit surface, was constant at the top of the track. The length of the track (in the x-direction) is much longer than the width of the track (in the y-direction) but for the purposes of our analysis we ignore edge effects due to the walls of the track.

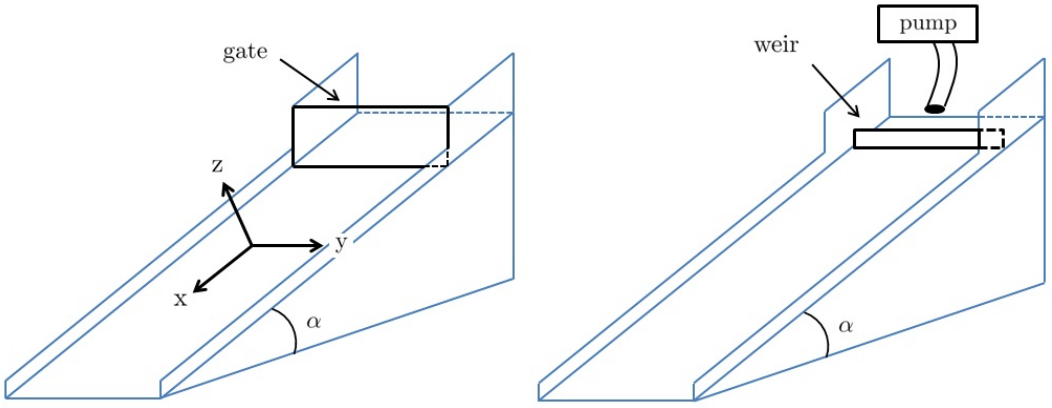

Figure 2: Schematic of our experimental setup. The left image depicts the setup for the constant volume experiments. The right image depicts the setup for the constant flux experiments. The coordinate system is kept constant for both initial conditions.

2.3. Analyzing the data

We quantified the positions of the fronts and the slurry's film thickness (height profile) along the x-axis. Both methods utilized code written in MATLAB, which is summarized in Appendix A. In order to find the position of the individual fronts, a camera was set up above the track with the face of the lens parallel to the plane of the track, 0.5 to 1 m away. The front position was computed for individual frames of the resulting video. Fronts are identified using RGB values for each vertical strip of the frame. We analyze multiple fronts since settled experiments have distinct front positions for the fluid and the two particle species. Figure 4 shows individual frames of a settled and well-mixed experiment.

We also investigated the film thickness of the flow along the x-axis (we present pseudocode in Appendix A). To do this, we first set up our camera next to the track such that the camera lens was pointed towards the track. The camera lens face was made to be perpendicular to the incline so that the camera could pick up the laser line deflection due to the calibration object and the slurry. We then shined a laser line on the middle of the track so that the line was parallel to the length of the track. Using calibration images of the empty track and of the track with an object of known height resting on it, we were able to process the video of the experiment to obtain the film thickness. As the slurry flowed down the track, the laser line's position in each frame was deflected by the presence of the slurry. This deflection was computed using MATLAB, in mm, which resulted in figures such as Figure 9.

3. Results

Our results are divided into three sections, based on the initial condition and the type of data presented: Section 3.1 (front tracking and regime classification for constant volume experiments), Section 3.2 (front tracking and regime classification for constant flux experiments), and Section 3.3 (film thickness for constant flux experiments). For each experiment, the inclination angle α, volume ratio χ, and total particle volume fraction ϕ were varied. Based on previous research, we expect the ridged regime for large α and ϕ and the settled regime for small α and ϕ.

3.1. Constant volume: front tracking and regime classification

We conducted experiments with a constant volume of slurry moving down an incline positioned at inclination angle, α, with particle volume ratio, χ. Pictures of the experiments are shown in Figure 3. With the exception of the $\chi = 0.5$ experiments, all experiments had a total volume fraction of $\phi = 0.45$. In terms of the regime that formed, the two angles produced different regimes for each χ value (see Table 2 for the classifications of the constant volume experiments). If we look at the two $\chi = 0.389$ experiments, the smaller angle produced a settled slurry while the larger angle produced a ridged slurry. Angle was not the only parameter that affected the regime. If we compare the top left experiment with the top right experiment and the bottom left experiment with the bottom middle experiment (in Figure 3), we see the volume fraction ratio and the total particle volume fraction also influenced the regime of the slurry. It appears that all three parameters—α, χ, and ϕ—affect the regime that is formed.

Figure 4 provides the evolution of two sample flows. In Figure 4a (a settled slurry), three distinct fronts formed for the PDMS, glass beads, and ceramic beads. In Figure 4b (a well-mixed slurry), the fluid and the particle fronts remained together. Using the front tracking technique described in Section 2.3 we produce the blue and green dots in Figure 4 which correspond to individual front positions. The leftmost two images of Figure 4a do not track the particle fronts well (this occurs in the beginning of most of our settled experiments due to variation of particle front color as the particles begin to settle). This error does not affect our analysis since theory

only predicts asymptotic behavior after the slurry has reached equilibrium (i.e. towards the end of the experiment) and thus front tracking early in the experiment is not as important as later on in the experiment. Notice that in Figure 4a, the fluid front moved faster than the particle fronts. With the angle and particle concentrations being so low, the particles settled to the bottom of the slurry (towards the incline surface) while the fluid flowed over the settled particles, moving faster. In Figure 4b, we no longer see this separation; the particles stayed well-mixed throughout the fluid.

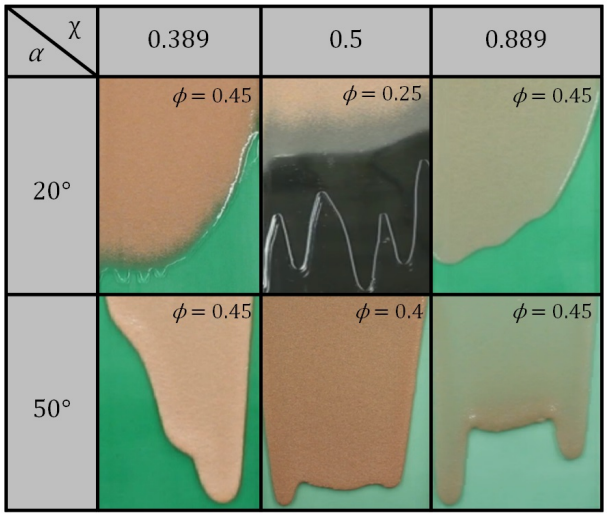

Figure 3: Experiments conducted with a constant volume of slurry. We perform six experiments total, with three different χ values (0.389, 0.5, and 0.889) and with two different angles (20° and 50°). The ϕ value for each experiment is also presented in the top right corner of each image. Note that the $(\chi, \alpha) = (0.5, 20°)$ experiment was conducted with a black background and all others were conducted with a green background.

α \ χ	0.389	0.5	0.889
20°	settled ($\phi = 0.45$)	settled ($\phi = 0.25$)	well-mixed ($\phi = 0.45$)
50°	ridged ($\phi = 0.45$)	well-mixed ($\phi = 0.4$)	ridged ($\phi = 0.45$)

Table 2: The six constant flux experiments presented in Figure 3 along with the observed regime and the total volume fraction of the fluid, ϕ.

According to theory, we expect the front position of the fluid to have behavior asymptotic to $t^{1/3}$, where t is time. This asymptotic behavior arises after the slurry has reached equilibrium so we fit the front position of the fluid to $x(t) = ct^{\beta} + k$ for constants c, k, and β when the slurry is approximately halfway down the incline. In Table 3, we present our fitted β values for each of our experiments presented in Figure 3. Notice that the settled experiments have fitted β values that are furthest away from our theoretical predictions. In these experiments, the fluid front separates from the particle front(s) and blends in with the incline making it difficult to track (see Figure 4a). Recall that for constant volume experiments, we expect the position of the fluid front to be asymptotic to $t^{1/3}$ after it reaches equilibrium. There is strong agreement between theoretical predictions and our non-settled experimental results and we suspect that we would

find better agreement for the settled experiments with either a different fluid color or a different front tracking method for settled experiments. In Figure 5a, we present our experimental data against the best fit line for the $(\chi, \alpha) = (0.389, 50°)$ experiment. For most constant volume experiments, the data fits well with the fitted equations. When we fit for β values with larger error, the experimental data does not align with the fitted equation as well as it does in Figure 5a.

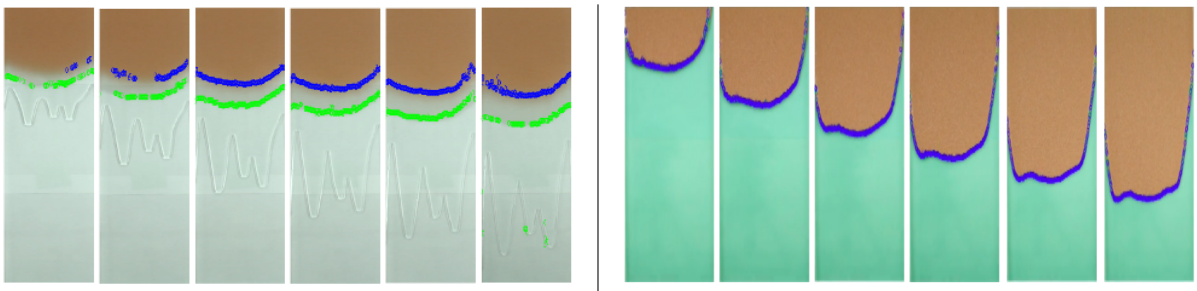

(a) $(\chi, \alpha) = (0.5, 20°)$ at 20 second intervals

(b) $(\chi, \alpha) = (0.5, 50°)$ at 12 second intervals

Figure 4: Processed video screenshots of the slurry flowing down the track. The light green and blue dots track the front position of the glass beads and ceramic beads, respectively. The left sequence of images are on a white background while the right sequence of images are on a green background.

α \ χ	0.389	0.5	0.889
20°	0.19 ± 0.5	0.22 ± 0.05	0.32 ± 0.05
50°	0.31 ± 0.02	0.39 ± 0.5	0.38 ± 0.07

Table 3: Fitted β values for each of the experiments presented in Figure 3 with their respective errors (95% confidence intervals).

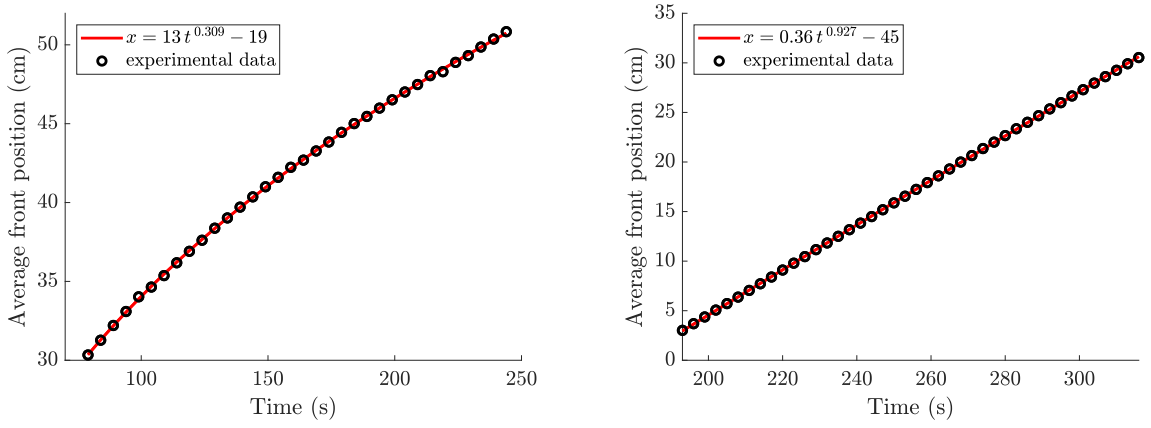

(a) constant volume fit

(b) constant flux fit

Figure 5: Fitted equations plotted against experimental fluid front data for a constant volume and a constant flux experiment, both of which are experiments in the ridged regime. (a) Corresponds to the $(\chi, \alpha) = (0.389, 50°)$ constant volume experiment while (b) corresponds to the $(\chi, \alpha) = (0.378, 50°)$ constant flux experiment.

3.2. Constant flux: front tracking and regime classification

We conducted eight constant flux experiments at different χ, α, and ϕ values, as shown in Figure 6. In each experiment we investigated the emergence of regimes, the front position, and film thickness (in Section 3.3).

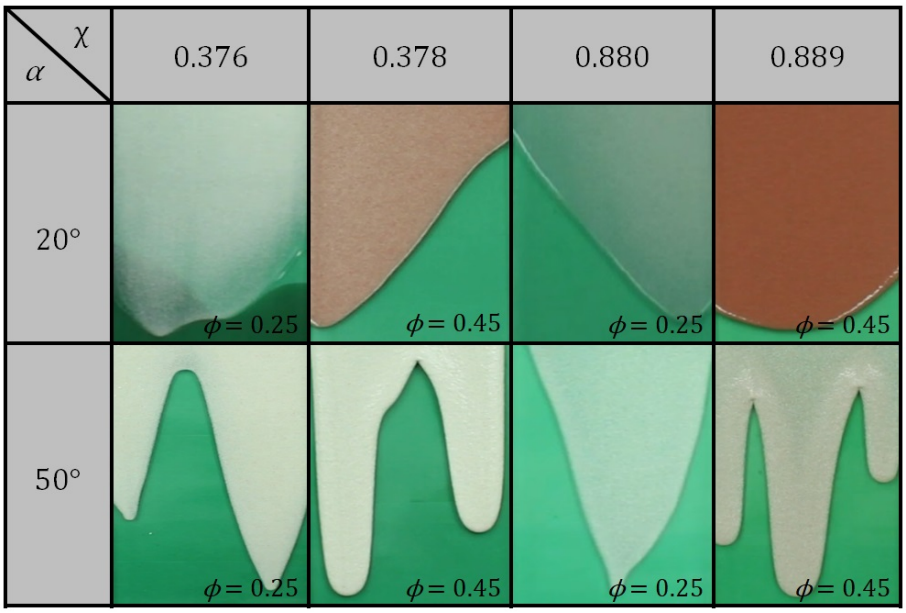

Figure 6: We performed eight constant flux experiments at four different χ values (0.376, 0.378, 0.880, and 0.889) and at two different inclination angles (20° and 50°). The ϕ value for each experiment is also presented in the bottom right corner. Each cell of the table is also classified by its regime in Table 4. Note that in only two of the experiments ($(\chi, \alpha) = (0.378, 20°)$ and $(\chi, \alpha) = (0.889, 20°)$) the ceramic particles are red and the glass particles are white while in the rest of the experiments both particle species are white.

Unlike constant volume experiments, we focus on two values of overall particle ratio ϕ: 0.25 and 0.45. For $\phi = 0.25$, the slurries are settled at $\alpha = 20°$, but at $\alpha = 50°$, the slurry is roughly well-mixed, possibly on the verge of a ridged regime. For $\phi = 0.45$ and $\alpha = 20°$, the slurries are well-mixed, possibly on the verge of a settled regime, while slurries at $\phi = 0.45$ and $\alpha = 50°$ are evidently ridged. While the volume fraction ratio χ affects the outcome, the angle of inclination α and the total volume fraction ϕ have a much larger effect on the regime produced. To see the regime classification of each of the experiments in Figure 6, see Table 4. The transient well-mixed regime occurred frequently, indicating that the experiment ended prematurely. A longer track would allow our slurry to flow further and might lead to different regime classification in these experiments.

α \ χ	0.376	0.378	0.880	0.889
20°	settled ($\phi = 0.25$)	well-mixed ($\phi = 0.45$)	settled ($\phi = 0.25$)	well-mixed ($\phi = 0.45$)
50°	well-mixed ($\phi = 0.25$)	ridged ($\phi = 0.45$)	well-mixed ($\phi = 0.25$)	ridged ($\phi = 0.45$)

Table 4: The eight constant flux experiments presented in Figure 6 along with the observed regime and the total volume fraction of the fluid, ϕ.

In addition to the regime formation we investigated the fluid front position of constant flux bidensity slurries. For these experiments we again attempted to fit the front position of our fluid to an equation of the form $x(t) = ct^{\beta} + k$ for some constants c, k, and β where we now expect our β value to be 1. We present our fitted β values in Table 5, where we see that the β values centered around 1. We obtain loose agreement with theoretical predictions, with the settled experiment $(\chi, \alpha) = (0.376, 20°)$ producing the result furthest from our predictions. Again, this is likely due to the fluid front being difficult to track once it separates from the particle front(s). We suspect that using a non-clear fluid or a different fluid front tracking method would produce stronger agreement in this settled experiment. To see an example fitted equation plotted against experimental data for a constant flux experiment, see Figure 5b.

α \ χ	0.376	0.378	0.880	0.889
20°	0.76 ± 0.3	0.90 ± 0.1	0.96 ± 0.1	0.91 ± 0.03
50°	1.1 ± 0.1	0.93 ± 0.09	1.18 ± 0.08	1.08 ± 0.09

Table 5: Fitted β values for each of the experiments presented in Figure 6 with their respective errors (95% confidence intervals). We expected our values to be around 1.

One interesting phenomenon that we saw in our experiments is presented in Figure 7. We noticed a folding-over phenomenon in constant flux experiments for large inclination angles and total volume fractions but never in other experiments. It was also only observed between fingers in these experiments (fingers correspond to the individual streaks of fluid that run down the track) and became most prominent towards the bottom of the track. The folding-over phenomenon started to form in the $(\chi, \alpha) = (0.889, 50°)$ experiment in Figure 6 and it developed into what we present in the right image of Figure 7.

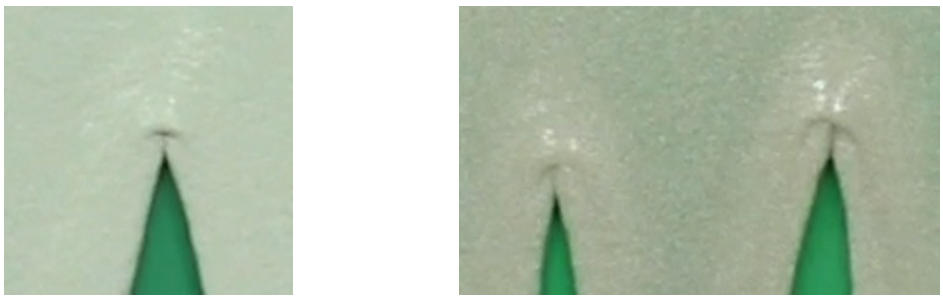

Figure 7: Two images of folding-over phenomenon occurring in constant flux experiments with large α and ϕ. Both images are zoomed in images from constant flux experiments with the left one corresponding to $(\chi, \alpha) = (0.378, 50°)$ and the right one corresponding to $(\chi, \alpha) = (0.889, 50°)$.

3.3. Constant flux: film thickness

To track the film thickness in each of the experiments presented in Figure 6, we implemented the film thickness tracking technique explained in Section 2. According to theory, we expect a distinct film thickness profile for each regime. We present the thickness of our fluid at four different times to show the evolution of the thickness for each of the three regimes in Figures 8, 9, and 10. We estimate the error in the measured film thickness to be about 0.5 mm (the film thickness should be smooth because of surface tension but error is introduced because of the resolution of our images). The sequences of images in Figures 8, 9, and 10 are characteristic of the thickness results for the settled, well-mixed, and ridged regimes, respectively. In most cases,

we found that the settled and well-mixed film thicknesses were similar: the smallest thickness was found at the front of the fluid and it increased after the front until a certain point where it would approximately plateau. This behavior is most clearly seen in the rightmost graph of Figures 8 and 9 although this behavior can also be seen in the other three graphs in the same figures. The ridged regime experiments, as predicted by theory, exhibited significantly different phenomena. In these experiments, the largest thickness was found at the very front of the fluid (which corresponds to the leading ridge of the slurry). Even from the very beginning of the experiment (the left two pictures of Figure 10) the ridge had already formed and continually led the fluid, although it did not necessarily grow higher or smaller during the experiment. We see the most pronounced ridge effect in the rightmost graph of Figure 10.

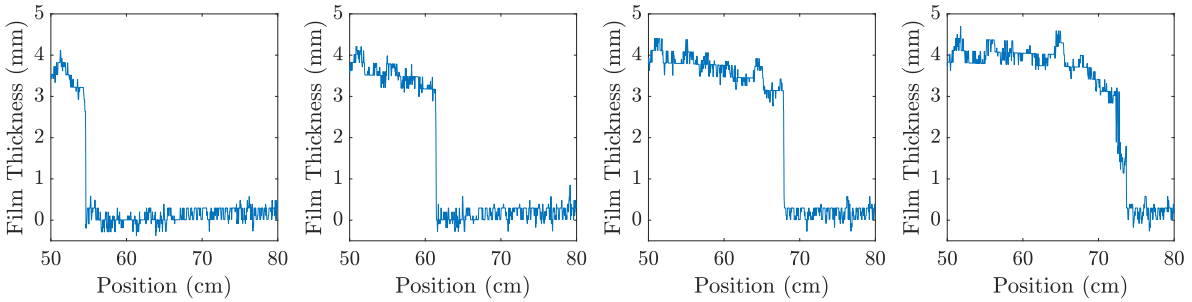

Figure 8: Film thickness of a constant flux slurry in the settled regime as it flows down an inclined track. These graphs correspond to the $(\chi, \alpha) = (0.880, 20°)$ experiment in Figure 6. The zero position is taken to be the location where the slurry starts to flow. Zero film thickness corresponds to positions on the track without slurry. The time between each consecutive graph is approximately 30 seconds.

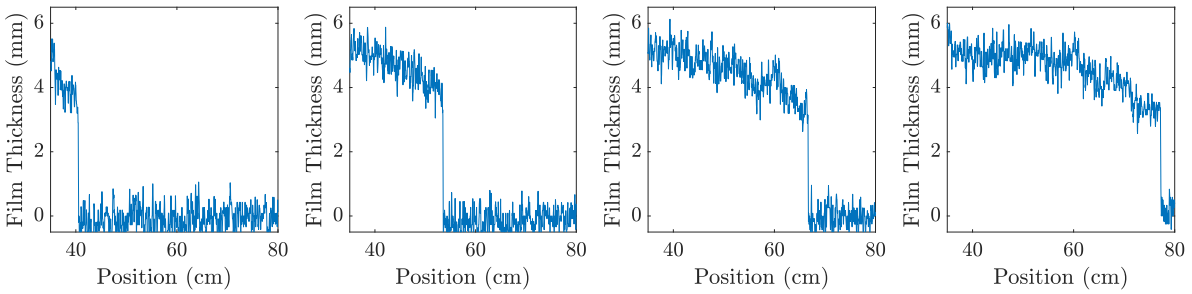

Figure 9: Film thickness of a constant flux slurry in the well-mixed regime as it flows down an inclined track. These graphs correspond to the $(\chi, \alpha) = (0.378, 20°)$ experiment in Figure 6. The zero position is taken to be the location where the slurry starts to flow. Zero film thickness corresponds to positions on the track without slurry. The time between each consecutive graph is approximately 1 minute.

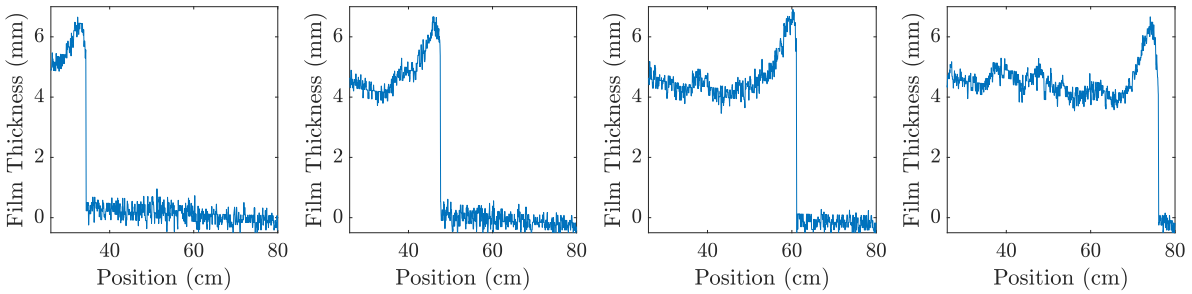

Figure 10: Film thickness of a constant flux slurry in the ridged regime as it flows down an inclined track. These graphs correspond to the $(\chi, \alpha) = (0.889, 50°)$ experiment in Figure 6. The zero position is taken to be the location where the slurry starts to flow. Zero film thickness corresponds to positions on the track without slurry. The time between each consecutive graph is approximately 1 minute.

4. Conclusion

We have extended the work presented in [5, 10, 11] to study both the constant volume and constant flux flows of bidensity slurries on an incline. Here, we have presented experiments that capture the regime and asymptotic behavior of bidensity particle-laden flows. Our regime results are well aligned with the predictions from previous research. Previous literature suggests that ridged slurries will form for large inclination angle, α, and large particle concentration, ϕ, while a settled regime will form for small α and small ϕ, which is what we see in Table 2. As expected, we see the transient well-mixed regime for small α and large ϕ as well as for large α and slightly lower ϕ. We find that experiments with the same α and ϕ but significantly different χ induced a change in regime, which corroborates one of the results from [10].

Since there is no previous literature on experimental constant flux bidensity slurries on an incline (to our knowledge), our experiments in this area are completely new. We expect the fluid front position to have linear asymptotic behavior (i.e. $x(t) = ct$, where c is some constant). Most of our fitted β values were close to the predicted value. Just as in the constant volume experiments, we note that the front tracking analysis often begins before the slurry has reached equilibrium due to the constraints in length of our track. Additionally, we expect the same pattern of regime formation as in the constant volume case, i.e. we expect that large α and ϕ will cause a ridged regime and small α and ϕ will cause the formation of a settled regime. We confirm this prediction experimentally, with one discrepancy: our results suggest that the well-mixed regime occurs approximately as frequently as the other two regimes combined, although this can be reconciled considering the length of our track.

The results of our film thickness experiments of constant flux slurries appear to be similar for the settled and well-mixed regimes. This similarity is unexpected. For the well-mixed regime, we expect to see a constant height wherever slurry is present due to the constant flux initial condition. However, we see a slight increase in height at the front of the slurry followed by a plateau in Figure 9. The discrepancy may be attributed to experimental error, or possibly surface tension. For the settled regime, we expect to see three distinct plateaus which correspond to the three fronts (see [5]). Two distinct plateaus are visible in Figure 8 but a third plateau is not distinguishable due to the resolution of our images. The slurries in the ridged regime had similar behavior to constant volume ridged slurries: a tall leading ridge at the front and an approximately constant plateau behind it.

We hope to continue this investigation. To directly extend the results of this study, more work should be done to determine the approximate length scale on which we expect to see the formation of our regime for constant flux experiments. With that information, we will be able to confirm whether or not the regime classification in Table 4 is correct. Additionally, we want to examine the unexpected folding-over phenomenon in Figure 7 in more depth to see if it only manifests in constant flux particle-laden slurries with large inclination angle and large total particle volume fraction. More broadly, theoretical studies on constant flux monodisperse and bidensity slurries could be conducted in order to match the theoretical front positions, regimes, and film thicknesses to experimental results. Work could also be done both experimentally and theoretically to understand the dynamics of bidisperse slurries flowing down an incline.

Acknowledgements

The authors would like to thank Professor Andrea Bertozzi and the team's mentors, Dr. David Arnold, Dr. Claudia Falcon, and Dr. Michael Lindstrom for their advice and guidance. This work was funded by NSF grant DMS-1312543.

REFERENCES

[1] B. P. Cook, A. L. Bertozzi, and A. E. Hosoi, *Shock solutions for particle-laden thin films*, SIAM Journal on Applied Mathematics **68** (2008), no. 3, 760–783.

[2] D. J. Arnold, Y. M. Stokes, and J. E. F. Green, *Thin-film flow in helically-wound rectangular channels of arbitrary torsion and curvature*, Journal of Fluid Mechanics **764** (2015), 76–94.

[3] F. de Rooij, *Sedimenting particle-laden flows in confined geometries*, Ph.D. thesis, University of Cambridge, 2000.

[4] H. E. Huppert, *Flow and instability of a viscous current down a slope*, Nature **300** (1982), no. 5891, 427429.

[5] J. T. Wong, and A. L. Bertozzi, *A conservation law model for bidensity suspensions on an incline*, Physica D: Nonlinear Phenomena **330** (2016), no. 1, 47–57.

[6] J. Zhou, B. Dupuy, A. L. Bertozzi, and A. E. Hosoi, *Theory for shock dynamics in particle-laden thin films*, Physical Review Letters **94** (2005), no. 11, 117803.

[7] L. Wang, A. Mavromoustaki, A. L. Bertozzi, G. Urdaneta, and K. Huang, *Rarefaction-singular shock dynamics for conserved volume gravity driven particle-laden thin film*, Physics of Fluids **27** (2015), no. 3, 033301.

[8] N. Murisic, B. Pausader, D. Peschka, and A. L. Bertozzi, *Dynamics of particle settling and resuspension in viscous liquid films*, Journal of Fluid Mechanics **717** (2013), 203231.

[9] N. Murisic, J. Ho, V. Hu, P. Latterman, T. Koch, K. Lin, M. Mata, and A. L. Bertozzi, *Particle-laden viscous thin-film flows on an incline: Experiments compared with a theory based on shear-induced migration and particle settling*, Physica D: Nonlinear Phenomena **240** (2011), no. 20, 1661–1673.

[10] S. Lee, A. Mavromoustaki, G. Urdaneta, K. Huang, and A. L. Bertozzi, *Experimental investigation of bidensity slurries on an incline*, Granular Matter **16** (2014), no. 2, 269–274.

[11] S. Lee, J. Wong, and A. L. Bertozzi, *Equilibrium theory of bidensity particle-laden flows on an incline*, Mathematical Modelling and Numerical Simulation of Oil Pollution Problems, Springer, 2015, pp. 85–97.

[12] S. Lee, Y. Stokes, and A. L. Bertozzi, *Behavior of a particle-laden flow in a spiral channel*, Physics of Fluids **26** (2014), no. 4, 1661–1673.

[13] T. Ward, C. Wey, R. Glidden, A. E. Hosoi, and A. L. Bertozzi, *Experimental study of gravitation effects in the flow of a particle-laden thin film on an inclined plane*, Physics of Fluids **21** (2009), no. 8, 083305.

Appendix A. Front position and film thickness codes

We present a pseudocode for how we compute the front position of each individual fluid and particle front in Algorithm 1. In front tracking experiments, we placed the camera above the incline with the lens face parallel to the incline. Our track had a middle section for the slurry to flow down and a left section with equally-spaced measurement lines (see Figure A.11a, a well-mixed slurry flowing down the incline). We present the cropped and rotated image of the slurry and measurement lines in A.11b. We present the same image with RGB values converted to HSV values and example clicks to find the maximum and minimum HSV values for each front in Figure A.11c. For a settled slurry, the user should click 10-15 times for each distinct front.

(a) unprocessed frame from *video*

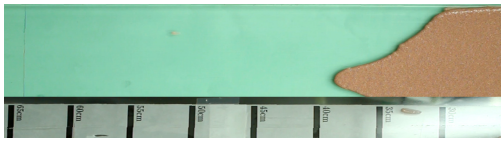

(b) rotated and cropped frame from *video*

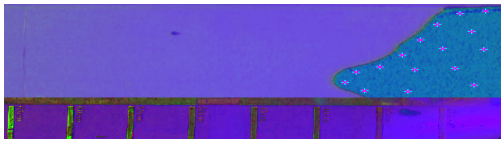

(c) HSV image with example clicking points

Figure A.11: Images used in our front tracking code. (a) is an unprocessed image of the slurry flowing down the incline with measurement lines next to the slurry. (b) is a rotated and cropped version of (a). (c) is the same as (b) but with RGB values converted to HSV values and example clicks.

We present a pseudocode for how we compute the film thickness (height profile) of our slurries in Algorithm 2. To see example images that the code uses, see Figure A.12. In these experiments, the camera must be in the same position for the *ref_image*, *cal_image*, and experimental *video*—next to the incline, with the camera lens face perpendicular to the incline so that the camera can pick up the laser line deflection due to the calibration object and the slurry.

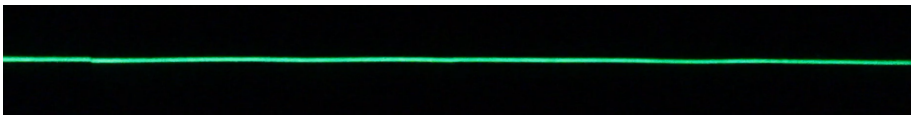

(a) example *ref_image*

(b) example *cal_image*

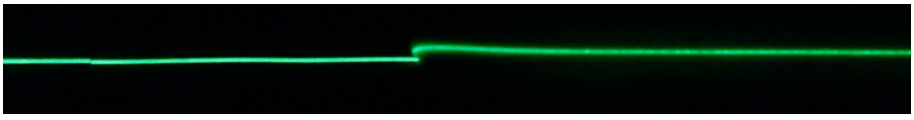

(c) example screenshot from experimental *video*

Figure A.12: Images used in the height profile (film thickness) code. The three images are all taken from the same position and the slurry in (c) is flowing from right to left.

Algorithm 1 Front Position

function FRONT_POSITION(*video*,*n*,*m*)
  input: *video* video of the slurry moving down the track (Figure A.11a)
    n number of frames to split the video into
    m number of fronts to process
  output: position of the front(s) over time

  function PROCESS_VIDEO(*video*,*n*,*m*)
    split the video into n equally-spaced frames
    for $i = 1, \ldots, n$ **do**
      rotate i^{th} frame such that the flow direction is pointing left
      crop i^{th} frame to only include the track and measurement lines (Figure A.11b)
      save i^{th} frame as *frame*(i)
    output: *frame*(1), . . . , *frame*(n)

  function IDENTIFY_FRONT(*frame*(1), . . . , *frame*(n), n, m)
    for $i = 1, \ldots, m$ **do**
      click at about 10-15 points in the i^{th} front in *frame*(n) (Figure A.11c)
      store the maximum and minimum HSV color value for i^{th} front
    for $i = 1, \ldots, n$ **do**
      let p = the number of horizontal pixel rows in *frame*(i)
      for $j = 1, \ldots, m$ **do**
        for $k = 1, \ldots, p$ **do**
          find left-most pixel in the k^{th} pixel row of *frame*(i) within j^{th} HSV range
          save x-position (horizontal pixel position) of left-most pixel to $P_x(i, j, k)$
    average $P_x(i, j, k)$ over the third index and save averages into $\bar{P}_x(i, j)$
    output: $\bar{P}_x(i, j)$

  function CONVERSION_AND_PLOT(*frame*(n))
    prompt user to click on the measurement lines in *frame*(n)
    assign length measurement to each measurement line click (0 cm, 5 cm, . . .)
    interpolate between clicks such that each pixel is assigned a length value
    convert $\bar{P}_x(i, j)$ from pixels to centimeters using result from previous line
    output: $\bar{P}_x(i, j)$ in centimeters

Algorithm 2 Film Thickness

function FILM_THICKNESS(*video*, *ref_image*, *cal_image*, *time_start, time_end, time_step*)
  input: *video* video of the experiment (Figure A.12c)
    ref_image image of laser beam on the clean track (Figure A.12a)
    cal_image image of laser beam with calibration object (Figure A.12b)
    time_start time when slurry front enters frame of video in seconds
    time_end time when slurry front leaves frame of video in seconds
    time_step time between frame samples in seconds
  output: film thickness in millimeters

  function CALIBRATION(*ref_image*, *cal_image*)
    extract undeflected laser line position from *ref_image* using pixel intensity
    linearly fit undeflected laser line position
    prompt the user to click the top of the calibration object in *cal_image*
    compute the pixel distance between the laser line fit and click
    equate calibration object thickness (in mm) and pixel distance for conversion factor
    output: *pixels_to_mm* pixels to mm conversion factor

  function HEIGHT(*video*, *ref_image*, *time_start*, *time_end*, *time_step*, *pixels_to_mm*)
    Split *video* into $n = \dfrac{(time\_end - time\_start)}{time\_step}$ frames
    for $i = 1, \ldots, n$ **do**
      rotate i^{th} frame and *ref_image* so that laser line is horizontal
      detect undeflected laser line position in *ref_image* using pixel intensity
      detect laser line position in i^{th} frame using pixel intensity
      compute laser line deflection in pixels between *ref_image* and i^{th} frame
      convert laser line deflection to mm using *pixels_to_mm*
      plot the laser line deflection in mm as the *film_thickness*
    output: *film_thickness* in millimeters